We are IntechOpen, the world's leading publisher of Open Access books Built by scientists, for scientists

6,900
Open access books available

185,000
International authors and editors

200M
Downloads

Our authors are among the

154
Countries delivered to

TOP 1%
most cited scientists

12.2%
Contributors from top 500 universities



WEB OF SCIENCE™

Selection of our books indexed in the Book Citation Index in Web of Science™ Core Collection (BKCI)

Interested in publishing with us?
Contact book.department@intechopen.com

Numbers displayed above are based on latest data collected.
For more information visit www.intechopen.com



Chapter 4

Polyadic Cantor Fractals: Characterization, Generation, and Application as Ultrasonic Lenses

Sergio Castiñeira-Ibañez, Daniel Tarrazó-Serrano,

José Miguel Fuster, Pilar Candelas and

Constanza Rubio

Additional information is available at the end of the chapter

http://dx.doi.org/10.5772/intechopen.68425

Abstract

The term fractal was coined in 1975 by Benoit Mandelbrot. Since then, fractal structures have been widely used by the international scientific community. Its range of applications includes multiple areas, such as optics, physics, cryptography, medicine, economics, and so on. The application of fractal structures to modulate light beams in the field of optics has been extensively studied, and it has been shown that in some cases these new fractal lenses improve the response of traditional lenses. Fractal lenses are able to provide beamforming capabilities, and allow the optimization of the optical beam according to the specific requirements. In some applications, it may be necessary to improve the focus in a certain area, while in others it may be critical to obtain a sharp attenuation by means of destructive interference. It may even be required a beam profile with multiple focus and a certain control over them. This work investigates the application of fractal structures based on Polyadic Cantor sets as ultrasonic lenses, analyzing how the relation between the different design parameters and the performance of the lens. It is shown that the working frequency becomes a precise control mechanism that can modify dynamically the focus position of the lens.

Keywords: fractal, polyadic Cantor sets, ultrasonic lenses, sound beam modulation, sound focusing

INTECH
open science | open minds

© 2017 The Author(s). Licensee InTech. This chapter is distributed under the terms of the Creative Commons Attribution License (http://creativecommons.org/licenses/by/3.0), which permits unrestricted use, distribution, and reproduction in any medium, provided the original work is properly cited. CC BY

1. Introduction

Every structure with symmetry properties of scale invariance, even for a short range, is likely to possess fractal properties. These structures are characterized by a noninteger fractal dimension that can be sighted as a measure of their irregularity. It can be said that the whole structure resembles its internal parts [1], and it has been found that several natural phenomena follow these patterns, such as snowflakes or some tree leaves. Fractal structures have attracted great interest from the scientific community, having been applied in several areas of science and technology, such as optic engineering, medicine, or economy [2]. Furthermore, research into the properties of heterogeneous artificial materials has been very active throughout the last two decades.

Wave application of fractal structures in the optical field has received a lot of attention, and it has been shown that the use of fractal diffractive lenses improve focalization over traditional lenses. These new fractal lenses have an interesting property, that is, they can produce multiple focal points along the optical axis due to the fact of fractal self-similarity [3].

Among other wave applications of fractal structures, different studies related to the acoustic field have been performed. Petri et al. [4] analyzed the vibration properties of a hierarchic system consisting on a Cantor sequence of piezoelectric and resin elements. Sapoval et al. [5] numerically investigated the acoustic properties of irregular cavities described as fractals. They proved that the geometric irregularity improved the modal density at low frequencies, localizing many of the modes at the edge of the cavity and modifying its attenuation properties. Lubniewski and Stepnowski [6] developed a simple method to identify the seabed using elements of fractal analysis. Castiñeira-Ibáñez et al. [7, 8] presented an acoustic barrier to control the noise formed by rigid cylinders in the fractal geometry of a Sierpinski triangle. These structures are capable of producing sharp attenuation by means of destructive interference, as well as focalization through constructive interference. Gomez-Lozano et al. [9] studied the transmission response in perforated plates with subwavelength holes. The transmission spectrums showed that every iteration with the Sierpinski carpet has the characteristic peaks and dips associated with the lattice constant of each matrix pattern. In other branches of acoustics, other devices based on diffraction such as root primary gratings (RPGs) offer the possibility of modulating acoustic beams.

Since the wave theory of different areas of physics have great similarity, many concepts used in these areas related to guiding the waves using fractal structures have been translated to the acoustic area and a new approach for the construction of ultrasonic lenses based on fractal structures is proposed. These lenses are able to modulate the ultrasonic beam in a different way compared to conventional lenses, where its ability to focus and guide waves comes from the fact that they are built with refractive materials with curved surfaces. Among different fractal structures, we have focused our attention on polyadic Cantor sets (PCSs). This type of fractals is very easy to construct, being that the main reason why most man-made fractal creations are based on Cantor fractals [10–17]. Nevertheless, focalization in the ultrasonic range requires further attention. Therefore, the aim of this chapter is to present the generation

http://dx.doi.org/10.5772/intechopen.68425

and characterization of fractal structures based on PCS and analyze their application as ultrasonic lenses.

2. Fractals

2.1. Fractal geometry

As it has been mentioned in Section 1, several phenomena in nature such as tree leaves, clouds, mountains, and circulatory system, among others, present fractal geometry (see **Figure 1**). Typical properties of fractal geometries, such as self-similarity, can be observed in these examples. The self-similarity property describes those fractals that contain self-copies and can be defined recursively. Thus, an object is said to be self-similar if its parts have the same shape or structure as the whole, although they may occur on a different scale and may also be slightly deformed. It is observed that the self-similarity property in elements in nature usually disappears after some iterations, not being able to reach infinity. When generating fractal structures, the current iteration of the fractal is also known as the stage of the fractal.

2.1.1. Fractal dimension

If the analyzed object presents self-similar properties, it can be considered a fractal object and thus it can be characterized by a parameter known as the fractal dimension (D).

Fractal dimension is a generic concept that has its origin in mathematical metrics. Unlike topological dimensions, the fractal dimension can take noninteger values. The topological dimensions of lines, squares, and cubes are respectively one, two, and three. Mandelbrot's research, based on previous works of Hausdorff, introduced the possible existence of geometric objects of intermediate dimensions between those integer values, and thus, the concept of fractal dimension [1, 18]. It can also be understood as a measure of the space-filling capacity of a fractal pattern.

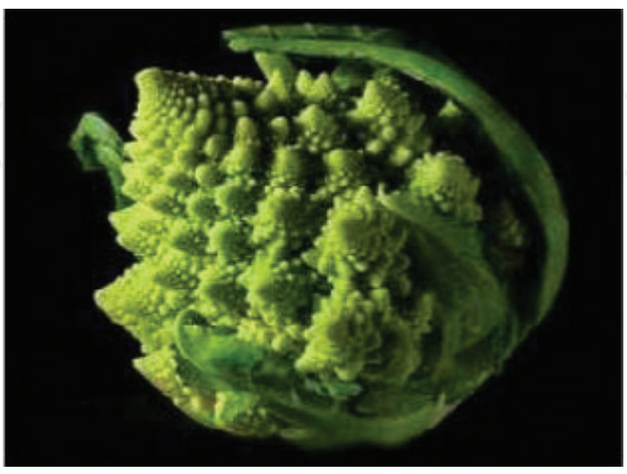


Figure 1. Example of fractal in nature (Public-Domain-Photos.com).

Fractals are generated from an initiator corresponding to step $s = 0$ (see **Figure 2**) and the fractal dimension can be calculated as,

$$D = -\frac{\ln N}{\ln r} \tag{1}$$

with N the number of self-copies of the initiator at stage 1 ($s = 1$), i.e., the generator and r the scale factor that rules the length shrinkage of the copy in each new stage.

This work focuses on a fractal structure based on the Cantor set. The original Cantor set is constructed, taking an initial unit segment at stage 0 ($s = 0$) and splitting it in three identical parts. Then, the middle segment is erased and the first stage ($s = 1$) is obtained. This procedure is repeated infinitely to obtain the Cantor set.

For the original Cantor set, the number of self-copies in stage $s = 1$ is $N = 2$, while the scaling factor becomes $r = 1/3$, resulting in a fractal dimension, which corresponds to a fractal dimension of $D = 0.6309$.

2.1.2. Lacunarity

In mathematics, symmetries are expressed as invariances, i.e., lack of change, under different operations such as a spatial translation. The concept of lacunarity was first used by Mandelbrot [1]. The lacunarity parameter was introduced to describe the degree of translational invariance or homogeneity of a fractal. It is a measure of how fractal patterns fill space. Patterns that present larger holes or show a lower translational invariance are generally said to have a high lacunarity. In contrast, fractals that are more homogeneous or approach translational invariance have low lacunarity. Thus, two fractals that are constructed with a similar procedure, and even have the same fractal dimension, may present a different lacunarity, depending on their degree of heterogeneity. It can be said that the lacunarity parameter, therefore, describes the texture of the fractal pattern and makes it possible to distinguish sets that have the same fractal dimension, but different textures [19].

Many methods have been proposed to quantify this fractal parameter, some of which involve calculating the first- and second-order moments of the fractal mass distribution. One of the best known methods is the gliding box algorithm that has been used in the present work.



Figure 2. Building of the Cantor set. Stages $s = 0$, 1, 2, and 3 are shown.

http://dx.doi.org/10.5772/intechopen.68425

2.1.3. Prefractal

As it has been explained in Section 2.1.1, fractals are generated from an initiator corresponding to step $s = 0$. In the next step ($s = 1$), the initiator is replaced by a number or scaled copies of itself. This procedure is repeated over and over in the following stages. Strictly speaking, a fractal is reached when the number of stages tends to infinity. When this whole process is truncated, prefractal structures are obtained instead.

However, throughout the chapter, the term fractal is used instead of the term prefractal as it has become a standard in engineering applications. However, this whole work refers to fractal structures with a finite stage of growth, i.e., prefractals.

2.2. Generalized polyadic Cantor sets

If the same construction procedure of the original Cantor set is replicated, but substituting the ratio $r = 1/3$ by an arbitrary ratio between 0 and 1/2, fractal sets with the same nature but with a different fractal dimension (D) are obtained. The fractal dimension has always a value between 0 and 1. These sets are known as generalized polyadic Cantor sets (GPCSs) and are characterized by the same parameters as the original Cantor set as shown in the **Figure 3** (s denotes the prefractal current stage; N, the number of scaled self-copies of the initiator at stage $s = 1$; D, the fractal dimension and, r, the scale factor with which each new copy is shrinked at the next stage). A new parameter ε represents the width lateral gaps generated at stage $s = 1$. This new parameter characterizes the distribution of the gaps inside the polyadic Cantor set and becomes a new design parameter, which enhances the control flexibility of these fractal structures in new applications. This ε parameter has also been widely accepted as an indication of the lacunarity parameter in the literature [15].

The size of all segments, which belong to the same stage (s) is identical and its value is ruled by the expression:

$$W_S = Lr^S \tag{2}$$

with L the length of the initial segment, i.e., the initiator.

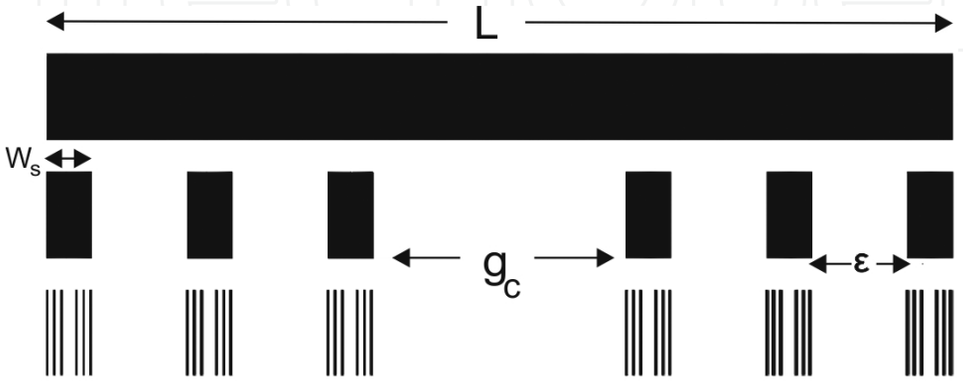


Figure 3. Generalized polyadic Cantor sets (GPCSs) main parameters.

Eq. (1), which calculates the fractal dimension, can be also expressed as a function of the number of gaps in stage 1 (n_{gaps}). Thus, the fractal dimension is rewritten as:

$$D = -\frac{\ln(n_{gaps} + 1)}{\ln r} \tag{3}$$

If the number of elements, N, is fixed, the scaling factor, r, must be modified to obtain a different fractal dimension, D. Thus, the fractal descriptor, D, becomes a direct measure of the transparency of the generated prefractal. If a prefractal presents a higher D parameter, it will be more opaque, i.e., filled with matter, whereas a lower D parameter results in a more transparent prefractal structure.

Generalized polyadic Cantor sets (**Figure 4**) can have either even or odd order. In the first stage ($s = 1$), the even-order sets have a central gap and an even number of gaps on both sides (lateral gaps). In contrast, those of odd order do not have a central gap, but two gaps or identical size next to the central segment. These two gaps closer to the center (adjacent gaps) are equivalent to the central gap in an even-order set. The rest of the gaps (lateral gaps) are identical among them and distributed as in the even-order case, but have a different size to the adjacent gaps.

The width of the central gap is denoted by g_C. In the even-order set the central gap has a width equal to $h\ g_C$, while in the odd-order case the two adjacent gaps have a width equal to $g_C/2$. The width of the lateral gaps for both the even case and the odd case is denoted by ε.

One can discuss which cases present minimal or maximum lacunarity. Thus, when all the gaps at the first stage, including the central or the adjacent gaps, are of equal width, the lacunarity is said to be minimal (homogeneous case). The value of this gap width, which produces this minimal lacunarity turns out to be:

$$\varepsilon_{min_lacunarity} = \frac{1 - N\,r}{N - 1} \tag{4}$$

As it can be observed in **Figure 5**, all of the gaps in stage $s = 1$ present the same width. This case is an even-order set with $N = 6$ and achieves minimum lacunarity since the distribution of gaps is homogeneous.

On the other hand, maximum lacunarity is achieved when the lateral gaps are removed ($\varepsilon_{max_lacunarity} = 0$). Thus, for an even-order Cantor set, a central gap remains in the middle of the set and two identical segments without gaps are placed at both sides of that central gap, as shown in **Figure 6**. For an odd-order cantor set, there is a segment in the center with two identical adjacent gaps. Then, two identical segments without lateral gaps are found at both sides of the set as in the even-order case.

Lacunarity may also be increased going in the opposite direction. The central gap may be shrinked instead of augmented. In this direction, the higher lacunarity is obtained when the central gap disappears and the whole gap space is split among the lateral gaps, as shown in **Figure 7**.

http://dx.doi.org/10.5772/intechopen.68425

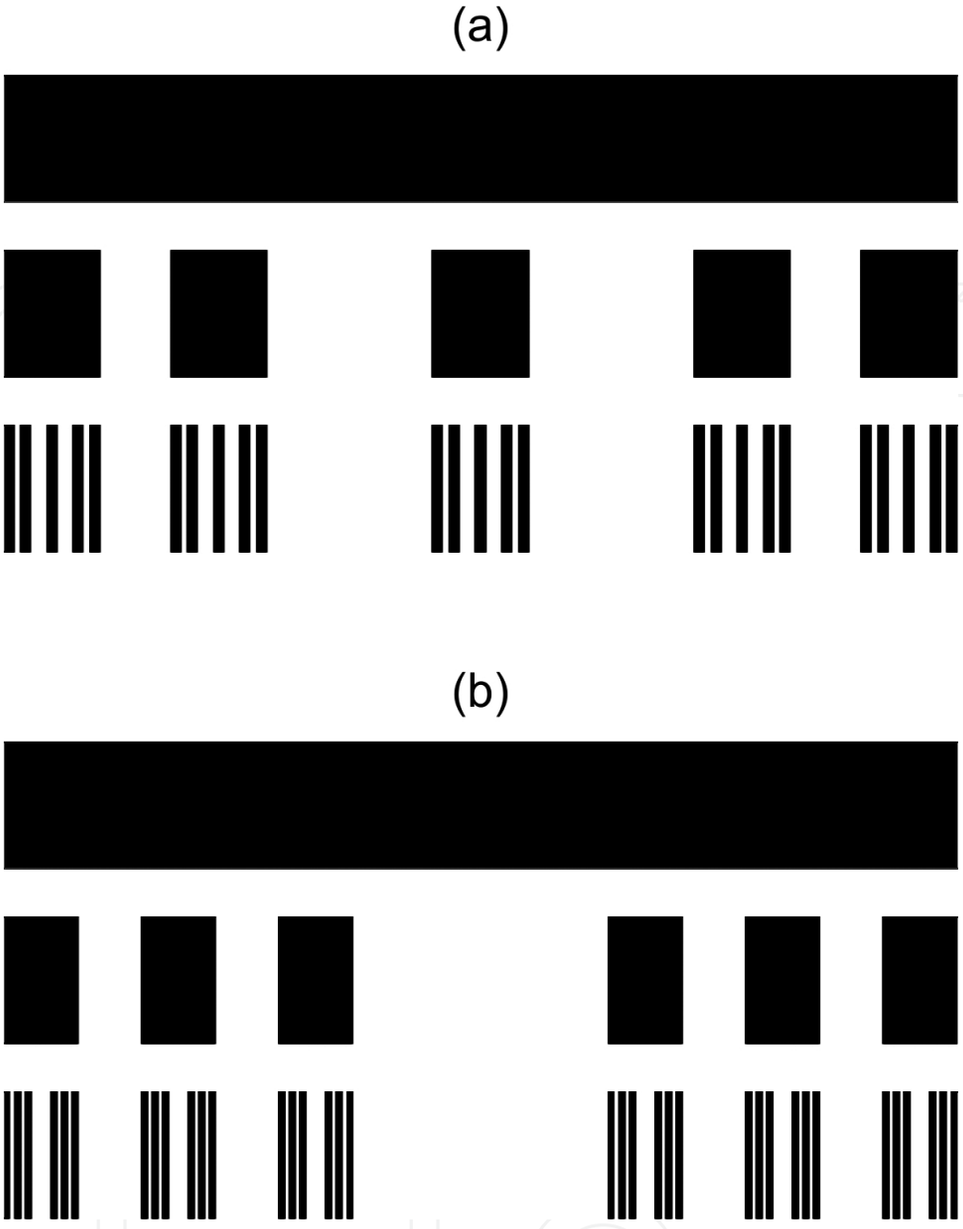


Figure 4. Generalized polyadic Cantor sets. (a) Odd order ($N = 5$) and (b) even order ($N = 6$).

This case corresponds to an ε value given by:

$$\varepsilon_0 = \frac{1 - N\,r}{N - 2} \text{ if } N \text{ is even} \tag{5}$$

$$\varepsilon_0 = \frac{1 - N\,r}{N - 3} \text{ if } N \text{ is odd} \tag{6}$$

The general expressions for the ε parameter, for any lacunarity value, are given by,

$$\varepsilon = \frac{1 - N\,r - g_C}{N - 2} \ (N \geq 4) \text{ if } N \text{ is even} \tag{7}$$

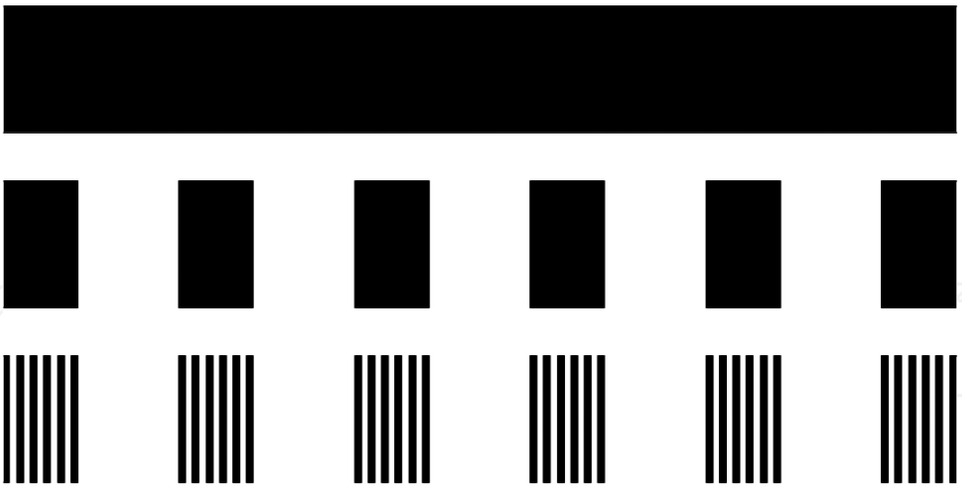


Figure 5. Generalized polyadic Cantor set ($N = 6$) with minimum lacunarity.



Figure 6. Generalized polyadic Cantor set ($N = 6$) with maximum lacunarity.

$$\varepsilon = \frac{1 - N\,r - g_C}{N - 3} \ (N \geq 5) \text{ if } N \text{ is odd} \tag{8}$$

Another very useful parameter is the central gap fraction (f_{gc}). This parameter conveys the same information as the ε parameter, but it is a more intuitive parameter easier to visualize. The central gap fraction represents the ratio between the width of the central gap and the total width of the combination of the gaps of the PCS. The central gap fraction can be expressed as,

$$f_{gc} = \frac{g_C}{1 - Nr} \ (N \geq 4) \tag{9}$$

And the relationship between the f_{gc} and the ε parameters is given by,

$$f_{gc} = \frac{1 - Nr - (N-2)\varepsilon}{1 - Nr} \text{ if } N \text{ is even} \tag{10}$$

http://dx.doi.org/10.5772/intechopen.68425

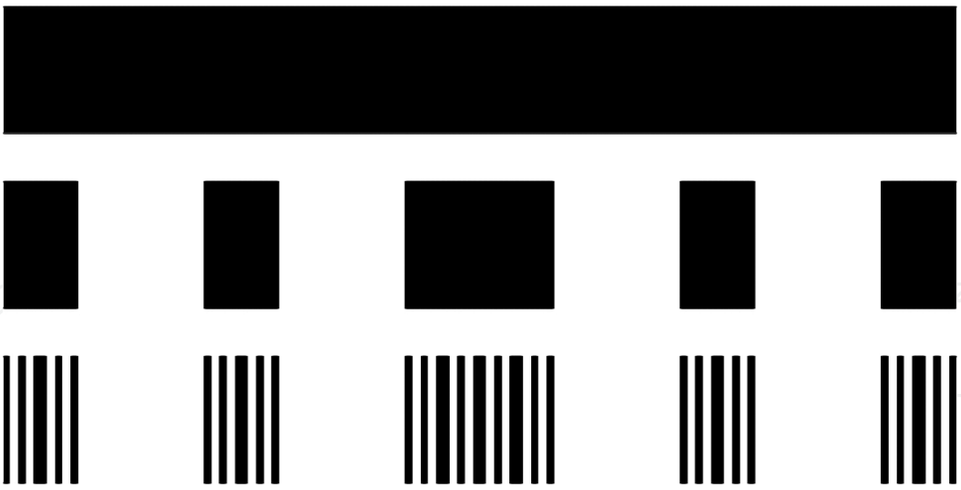


Figure 7. Generalized polyadic Cantor set ($N = 5$) with high lacunarity.

$$f_{gc} = \frac{1 - Nr - (N-3)\varepsilon}{1 - Nr} \text{ if } N \text{ is odd} \tag{11}$$

3. Numerical models and lens design

The interaction of acoustic waves with matter is well explained by means of theoretical models. The development of these accurate models has allowed, to a large degree, the development of acoustics in the last decades. These models are numerically programmed, providing an intake to understand the underlying physics in new systems and devices. Thus, numerical modeling is a very useful tool to enhance the design of polyadic Cantor fractal lenses (PCFLs) before fabricating them.

In our work, numerical modeling has been split into two separate procedures. First, polyadic Cantor sets and their corresponding ultrasonic lenses are designed using the Matlab software, and then, their acoustic behavior has been analyzed using the finite element method (FEM).

The main parameters used for the design of the PFCL are the following: fractal dimension (D), stage (s), number of self-copies of the generator (N), central gap fraction (f_{gc}), scale ratio (r), central gap width (g_C), and lateral gap width (ε). Additionally, there are other parameters that also affect the behavior of the lens and have to be considered, such as the working frequency (f) or the size of the lens characterized by its radius (R).

The scale ratio can be easily obtained from Eq. (1) and is given by,

$$r = N^{-1/D} \tag{12}$$

And the central gap width can be calculated from,

$$g_C = (1 - rN) f_{gc} \tag{13}$$

The following equations show the theoretical formulas to calculate the position of the Cantor bars in a polyadic Cantor set. These equations are implemented recursively. The first stage is

calculated using Eq. (14) and has a different implementation depending on the order (even or odd) of the PCS. The rest of the stages are computed recursively from stage $s = 1$ using Eq. (15).

$b_{(i,1)}$ indicates the start and end of each of the Cantor bars in stage $s = 1$, where i is an integer index that ranges from 1 to $2N$.

$$b_{(i,1)}\begin{cases} \text{int}\left(\frac{i}{2}\right)\cdot r + \text{int}\left(\frac{i-1}{2}\right)\cdot \varepsilon + \text{true}(i > N)(g_C - \varepsilon) \text{ even } N \\ \text{int}\left(\frac{i}{2}\right)\cdot r + \text{int}\left(\frac{i-1}{2}\right)\cdot \varepsilon + \text{true}\left(i > (N-1)\right)\left(\frac{g_C}{2} - \varepsilon\right) + \\ \qquad + \text{true}\left(i > (N+1)\right)\left(\frac{g_C}{2} - \varepsilon\right) \text{ odd } N \end{cases} \tag{14}$$

In Eq. (14), the function int(x) stands for the floor function that maps a real number to the largest previous integer and the function true(x) is the true function which returns the value 1 when the condition inside the brackets is fulfilled and 0 otherwise.

$b_{(i,s)}$ indicates the start and end of each of the Cantor bars in stage s, where i is an integer index that ranges from 1 to $2N^s$.

$$b_{(i,s)} = b\left(1 + 2\,\text{int}\left[\frac{i-1}{2N^{s-1}}\right], 1\right) + r\cdot b(1 + \text{mod}[i-1, 2N^{s-1}],\ s-1) \tag{15}$$

The function mod(x,y) returns the reminder after division x by y.

Once the polyadic Cantor sets have been constructed, box counting methods have been used to verify the main fractal parameters, which are fractal dimension and lacunarity.

PCS have axial symmetry, and this symmetry is extended to the construction of its corresponding lens. The PCFL is constructed by rotating the PFS around its symmetry axis. When using the finite element method to simulate the PCFL acoustic behavior, this symmetry becomes a significant advantage as it reduces the computational time of the simulation.

Describing physical phenomena frequently leads to space and time-dependent problems, mathematically described by partial differential equations (PDEs). In the PFCL characterization, it is not possible to solve these equations analytically and a numerical approximation, typically, in terms of a certain discretization, is applied. FEM have been conceptually developed for the numerical discretization of problems with bounded domains and they are especially applicable for solving Helmholtz problems. A PCFL characterization problem in which the geometry, boundary conditions, and materials are symmetric with respect to an axis can be solved as an axisymmetric problem instead of as a three-dimensional problem.

The interaction of ultrasound waves with ultrasonic lenses is a very complex problem. The finite element method (FEM) seems to be an appropriate computational tool to determine the distribution of acoustic pressure and, therefore, the focal position and the size of the focal spot. To decrease the computational cost of the simulations, the geometrical properties of the model that has been implemented must be taken into account. Due to axial symmetry of these

http://dx.doi.org/10.5772/intechopen.68425

structures, numerical calculation was made by means or the 2D axisymmetric method. This model includes a piston source, which consists of an axially oscillating disk of dimensions equal to the axisymmetric lens. A plane wave with amplitude P_0 impinges the axisymmetric lenses upward along the y-direction.

For this purpose, it is necessary to solve the Helmholtz equation given by

$$\nabla\left(-\frac{1}{\rho}\nabla p\right) = \frac{\omega^2}{\rho c^2} p \tag{16}$$

where ρ (ρ = 1000 kg/m^3) is the medium density, c (c = 1500 m/s) is the ultrasound velocity, ω is the angular frequency, and p is the acoustic pressure. The assumptions made in the simulations are the following: (1) the wavelength of the incident plane wave (IPW) is large compared to the thickness of the lens, (2) the lens is considered to be acoustically rigid, therefore, the Neumann boundary condition (zero sound velocity) is applied, and (3) the plane wave radiation condition is applied to the boundaries of the domain to simulate free space and emulate the Sommerfeld condition in the numerical solution of the wave problem as shown in **Figure 8**.

Due to the characteristics of the system that is being modeled, where small time-dependent pressure variations values are assumed, the so-called background pressure field is considered.

To quantify the acoustic field, the sound pressure level is calculated in each point of the domain, and then the acoustic gain is calculated using the expression

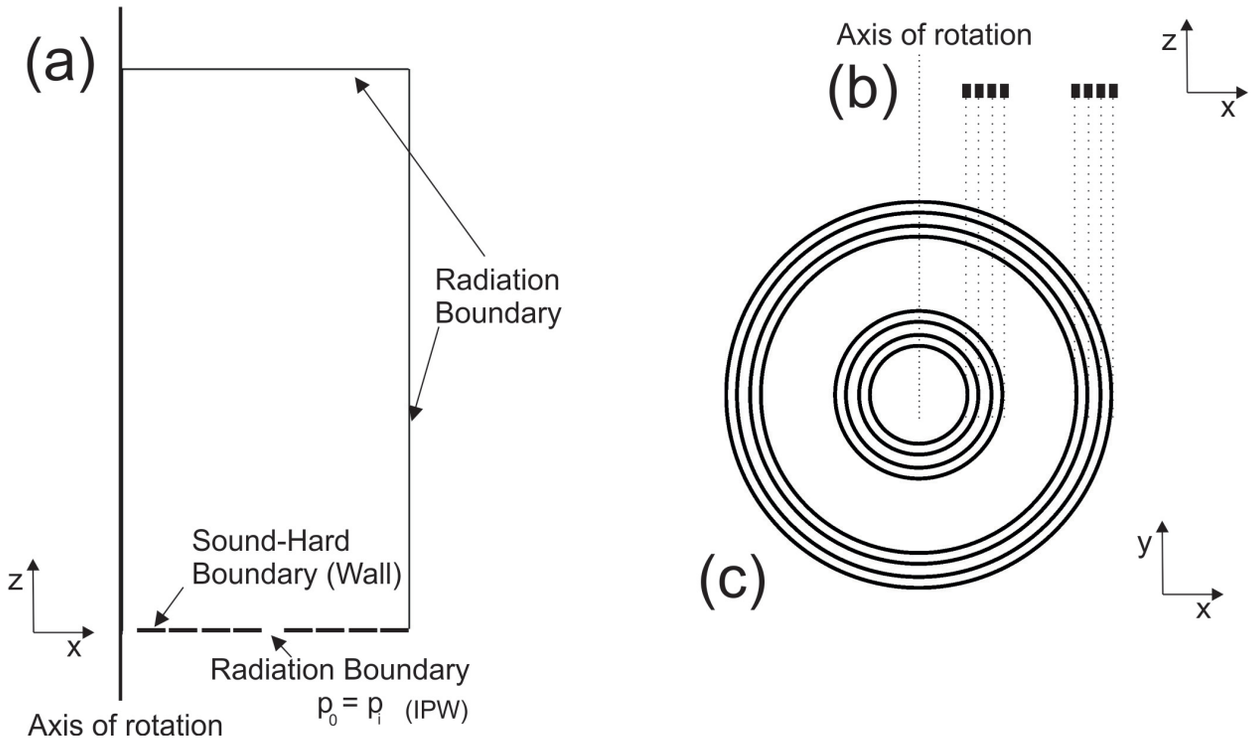


Figure 8. (a) Schematic diagram of the configuration simulated in the numerical domain where the solutions are obtained. (b) *XZ*-plane view of the PCFL. (c) *XY*-plane view of the PCFL.

$$G_{\text{focus}} = 20 \cdot \log_{10} \left| \frac{p}{p_{\text{incident}}} \right| \tag{17}$$

where p is the sound pressure at an arbitrary point, and p_{incident} is incident pressure at the lens.

4. Characterization of polyadic Cantor fractal lenses

Once the design parameters of the polyadic Cantor fractal lenses (PCFLs) have been presented, the influence of these parameters onto the modulation of sound beams is analyzed using the numerical method described in the previous section. All this work is applied to design acoustic lenses with beamforming and focal energy control mechanisms.

As it can be observed from **Figure 9**, a source emits waves of a certain frequency generating an incident plane wavefront (IPW) traveling in the direction of the *Z*-axis. The lens is oriented parallel to the *XY* plane ($Z = 0$), and is intercepted by this IPW. The PCFL has several rings that, due to diffraction phenomena, produce an infinite number of in-phase emission points, which generate a certain beamforming of the sound beam. In particular, much of the energy is concentrated at a point known as the focal lens (FL), because of constructive interferences. These types of lenses may generate more than one focus along the *Z*-axis, depending on the selected parameter values, and that can become an advantage in certain applications.

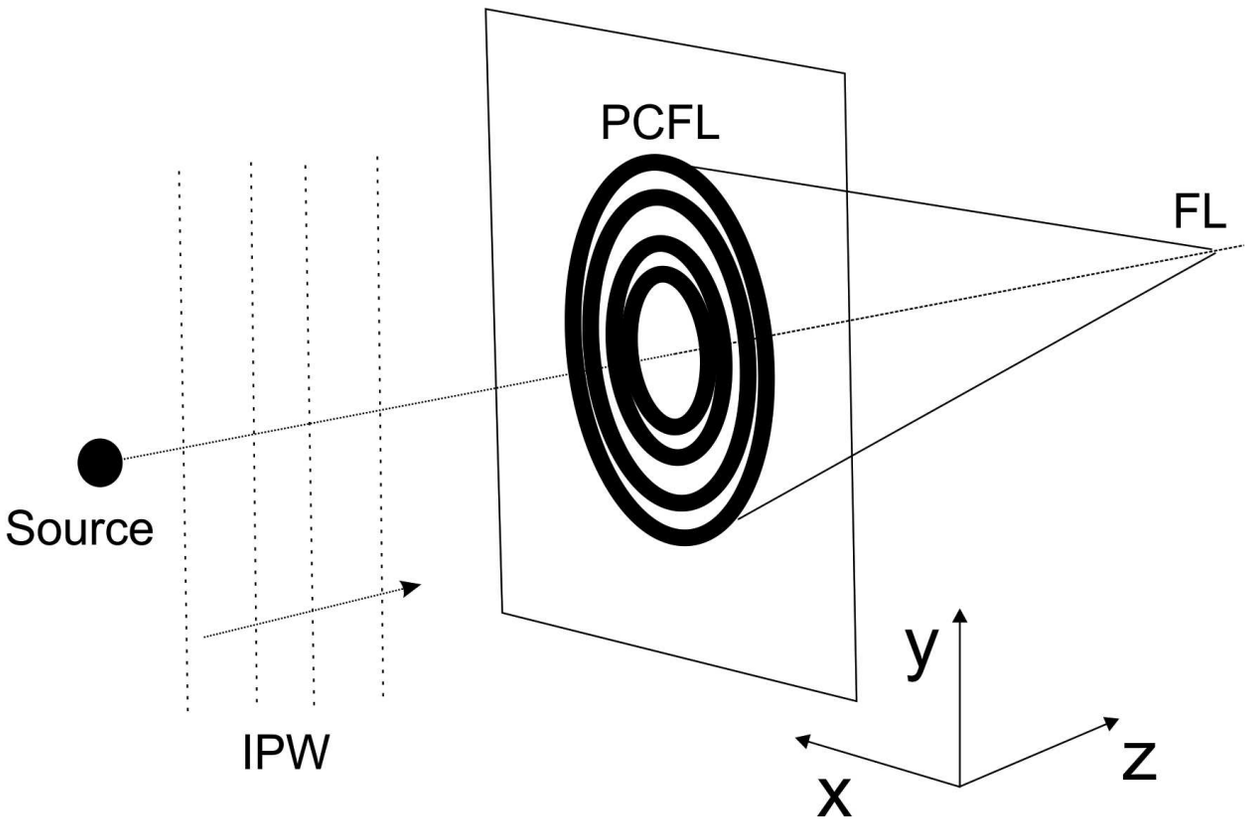


Figure 9. Numerical set-up. The IPW and FL are in *Z*-axis direction and the PCFL is placed in the *XY*-plane.

http://dx.doi.org/10.5772/intechopen.68425

The final objective of this work is two-fold. On the one hand, the design of fractal lenses, which are capable of modulating the acoustic beam, is pursued. On the other hand, once a specific lens has been designed, it is desirable to find a dynamic parameter, such as the working frequency, that allows a certain control on the beamforming capabilities of the lenses.

For this purpose, a lens of R = 12.5 cm and negligible thickness, compared to the working wavelength, is selected. The design parameters are initially set to the following values: D = 0.6, N = 5, f_{gc} = 0.4. The working frequency is set to f = 100 kHz. For practical reasons, the PCFL stage will remain constant with value s = 2.

Throughout this section, each of the design parameters (f, D, f_{gc}, and N) will be shifted to different values, one parameter at a time, keeping the remaining parameters to their initial values. With this procedure, the influence of each parameter onto the acoustic response of the designed PCFL can be analyzed independently. Likewise, a similar study is carried out to establish the effect of the working frequency on the beamforming capability of the PCFL.

4.1. Focal distance variation with frequency

Using the design parameters values given above (D = 0.6, N = 5, f_{gc} = 0.4, s = 2, and R = 12.5 cm), a PCFL has been simulated using to the numerical methods discussed in Section 3. A flat acoustic wavefront reaches the lens. The frequency of this wavefront is shifted to values between 50 and 400 kHz. The effect of the frequency shift onto the acoustic transmission variation and beamforming modulation is then analyzed. The PCFL in the XZ-plane view is shown in **Figure 10**. **Figure 11** shows the pressure maps (gains in dB) at the XZ-plane, perpendicular to the wave propagation direction, for frequencies of 50, 100, 200, 300, and 400 kHz.

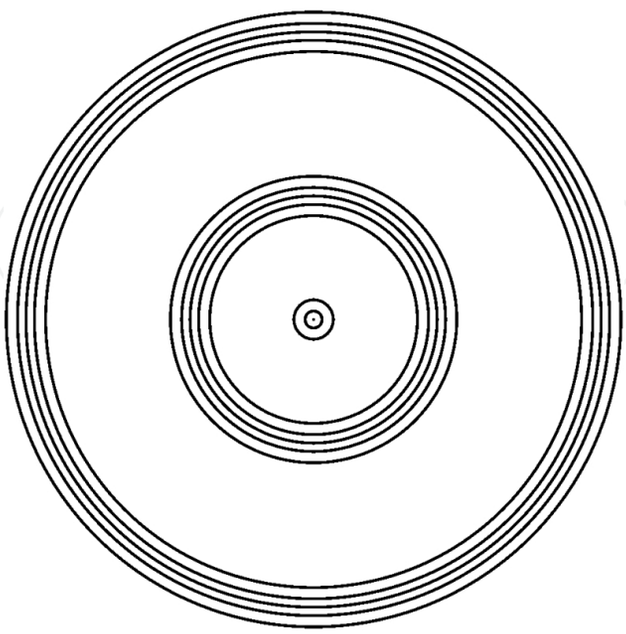


Figure 10. XY-plane view of the PCFL with D = 0.6, N = 5, f_{gc} = 0.4, s = 2, and R = 12.5 cm.

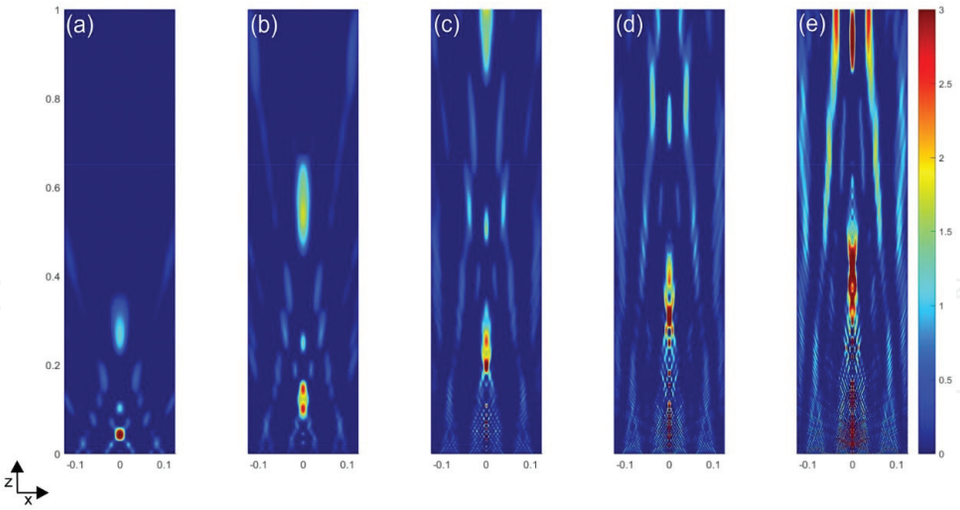


Figure 11. Two-dimensional spatial distribution of the acoustic gain (in dB) in the *XZ*-plane for the PCFL with $D = 0.6$, $N = 5$, $f_{gc} = 0.4$, $s = 2$, and $R = 12.5$ cm, for (a) 50 kHz, (b) 100 kHz, (c) 200 kHz, (d) 300 kHz, and (e) 400 kHz.

Analyzing the variation with the *X*-axis, direction parallel to the lens, a focalization in the central region ($x = 0$) may be observed. This focalization is constant and independent of the working frequency. However, the variation with the *Z*-axis, direction perpendicular to the lens, is a different subject. It can be observed that the position of the focalization area shifts with the working frequency. Moreover, the focalization area width and the focal gain also increase with the working frequency. From the simulation, a linear relationship can be established between the PCFL focal length and the working frequency given by:

$$d_f = d_{50}\frac{f}{50} = kf \tag{18}$$

being d_{50} the distance from the closest focus to the lens at a frequency of 50 kHz, which has been considered as the reference frequency, in *m*, f is the current working frequency in kHz, and d_f is the focal distance for the current working frequency in m. The k factor is defined to simplify the expression as the ratio between the focal distance at the reference frequency and the value of that reference frequency in kHz. This constant has been defined in m/kHz units.

This result is very significant, since it allows a very precise control of the lens focus location in a dynamic way, without requiring the modification of the lens design. In medical applications where focal location control is critical, such as thermal, these types of lenses have a great potential. They can be combined with high-intensity focus ultrasound (HIFU) to design treatment planning and targeting before applying an ablative level of ultrasound energy.

4.2. Variation of the fractal dimension *D*

In order to analyze the influence of the fractal dimension on the PCFL design, the design parameters are reboot to the initial values that have been previously selected ($N = 5$, $f_{gc} = 0.4$, $s = 2$, $R = 12.5$ cm) and the working frequency is set to $f = 100$ kHz. The *XZ*-view of the PCFLs for different values of *D*, (a) $D = 0.5$, (b) $D = 0.6$, (c) $D = 0.7$, and (d) $D = 0.8$, are shown in

http://dx.doi.org/10.5772/intechopen.68425

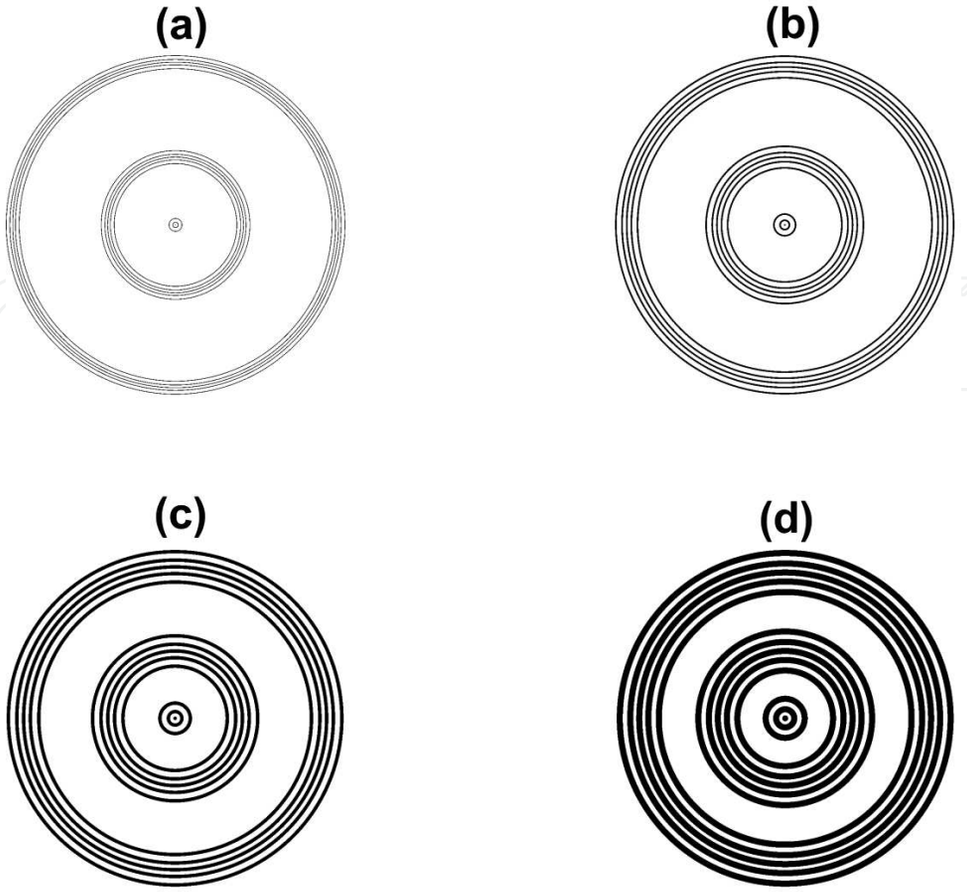


Figure 12. *XY*-plane view of the PCFL with $N = 5$, $f_{gc} = 0.4$, $s = 2$, and $R = 12.5$ cm and $f = 100$ kHz for: (a) $D = 0.5$, (b) $D = 0.6$, (c) $D = 0.7$, and (d) $D = 0.8$.

Figure 12. It can be observed how the lens becomes more opaque as D increases. **Figure 13** shows the pressure maps (gain in dBs) for fractal dimension values of $D = 0.5$, 0.6, 0.7, and 0.8.

Figure 13 shows that the focus position remains constant with the fractal dimension, and there is not any shift in either the *X*- or the *Z*-axis directions. However, the fractal dimension value has an influence on the focal gain of the PCFL. This effect is due to the diffraction mechanism. The raise on fractal dimension results in a more opaque lens, and the transmitted wave decreases, while the diffracted field increases, resulting in higher constructive interference at the lens focuses. The required focal gain will depend on the specific application and will define the fractal dimension for the PCFL design, as described in Section 4.1.

4.3. Variation of the central gap fraction (f_{gc})

In this section, the influence of the central gap fraction parameter (f_{gc}) on the PCFL beamforming capabilities is analyzed. The rest of the parameters are set again to their initial values (f = 100 kHz, N = 5, s = 2, D = 0.6, and R = 12.5 cm) as in the previous cases. From **Figure 14**, it can be noted how as the f_{gc} parameter increases the central gap width increases and then, the lateral gap width decreases. **Figure 15** shows the PCFL pressure maps (gain in dB) for f_{gc} values: (a) $f_{gc} = 0.2$, (b) $f_{gc} = 0.4$, (c) $f_{gc} = 0.6$, and (d) $f_{gc} = 0.8$.

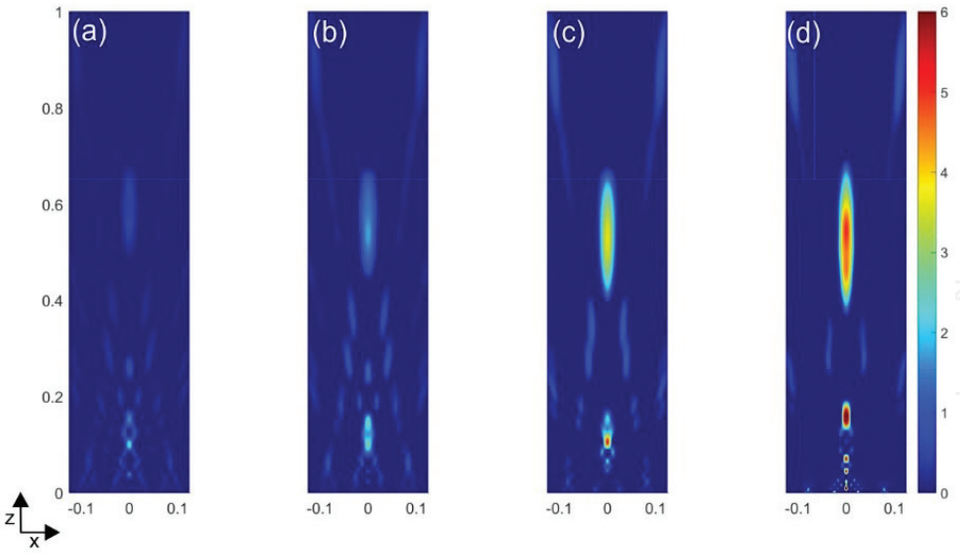


Figure 13. Two-dimensional spatial distribution of the acoustic gain (in dB) in the *XZ*-plane for the PCFL with $N = 5$, $f_{gc} = 0.4$, $s = 2$, and $R = 12.5$ cm and $f = 100$ kHz for: (a) $D = 0.5$, (b) $D = 0.6$, (c) $D = 0.7$, and (d) $D = 0.8$.

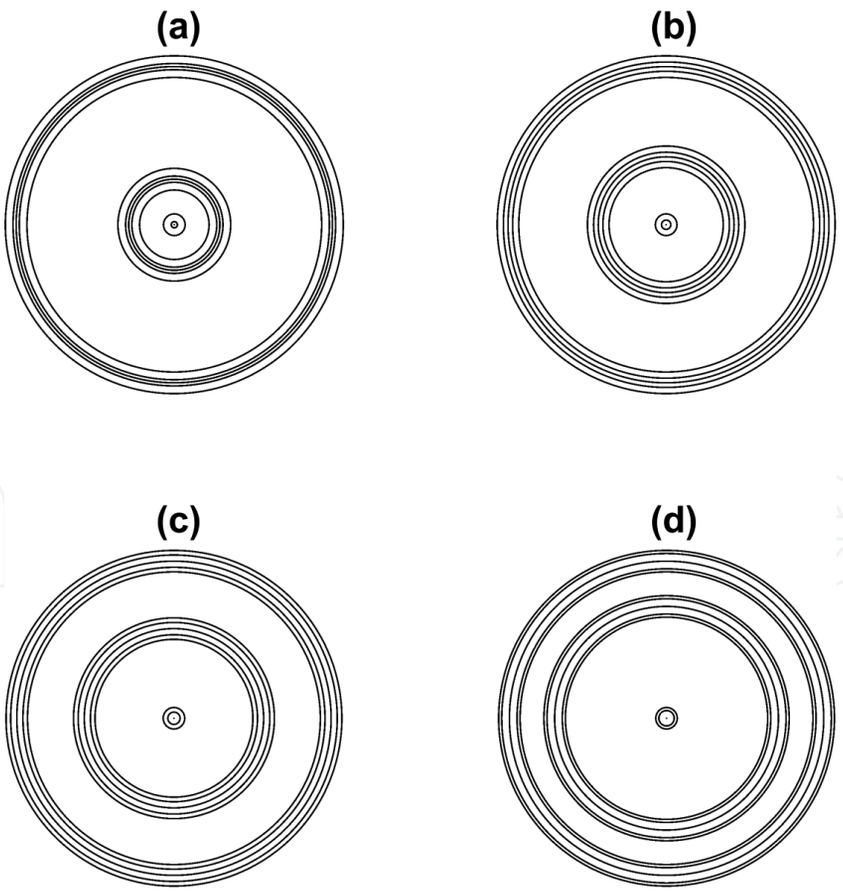


Figure 14. *XY*-plane view of the PCFL with $N = 5$, $D = 0.6$, $s = 2$, and $R = 12.5$ cm and $f = 100$ kHz for: (a) $f_{gc} = 0.2$, (b) $f_{gc} = 0.4$, (c) $f_{gc} = 0.6$, and (d) $f_{gc} = 0.8$.

http://dx.doi.org/10.5772/intechopen.68425

The increase of the f_{gc} parameter results in a larger central gap, while the lateral gaps width (ε) becomes smaller, remaining constant the combination of the widths of all the gaps present in the PCFL. The ε parameter has been previously defined in Eqs. (7) and (8).

Figure 15 shows the influence of the central gap fraction on the modulation of the acoustic beam. It can be shown that the focal points remain at the same locations. At the further focus, approximately located at z = 0.55 m, the focal gain diminishes when the f_{gc} parameter is increased, while the closest foci increase their focal gain with the f_{gc} parameter. Therefore, the f_{gc} selection has a direct impact on the modulation of the acoustic beam and should be carefully considered when designing the PCFL.

4.4. Variation of the number of elements (*N*)

In this section, the influence of the N parameter on the pressure maps is considered. The rest of the parameters are set to their initial values as in the previous sections (f = 100 kHz, s = 2, D = 0.6, f_{gc} = 0.4 = 0.4, and R = 12.5 cm). **Figure 16** shows the XY-plane views of the PCFLs for different N values (N = 4, 5, 6, and 7) while **Figure 17** shows their corresponding pressure maps.

Table 1 shows the dependence of parameters r and g_C with N. Increasing N results in a decrease in r if fractal dimension is kept constant, as a result of the elements becoming smaller. However, this inverse relationship is not linear as can be observed in Eq. (1). Therefore, the opaque percentage of the PCFL diminishes when N is increased, and the central gap becomes higher. Thus, increasing the number of elements N makes the lens slightly more transparent without requiring the variation of the fractal dimension.

Figure 17 shows a similar behavior to that obtained in Section 4.3, reducing the focal gain of the further focus and increasing the focal gains of the closest foci when the number of elements is increased.

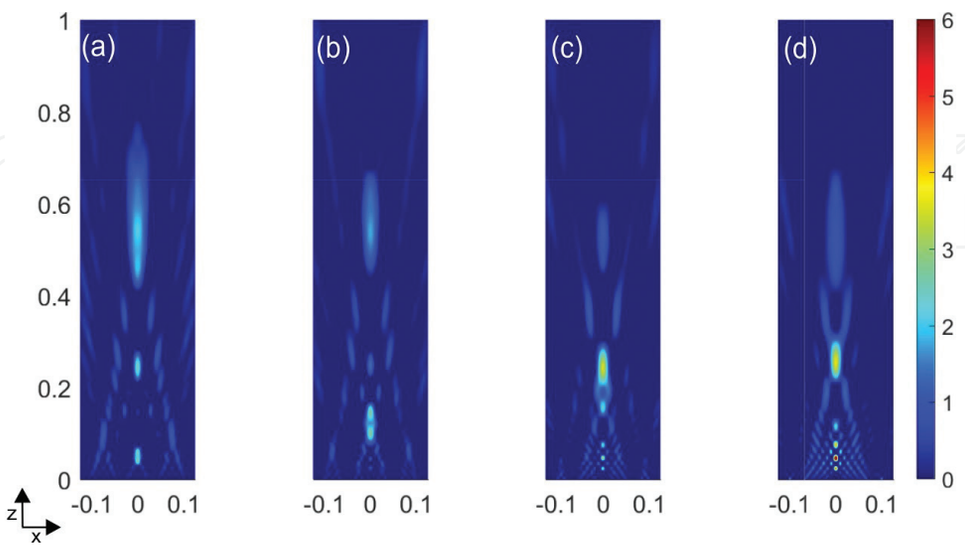


Figure 15. Two-dimensional spatial distribution of the acoustic gain (in dB) in the XZ-plane for the PCFL with N = 5, D = 0.6, s = 2, and R = 12.5 cm and f = 100 kHz for (a) f_{gc} = 0.2, (b) f_{gc} = 0.4, (c) f_{gc} = 0.6, and (d) f_{gc} = 0.8.

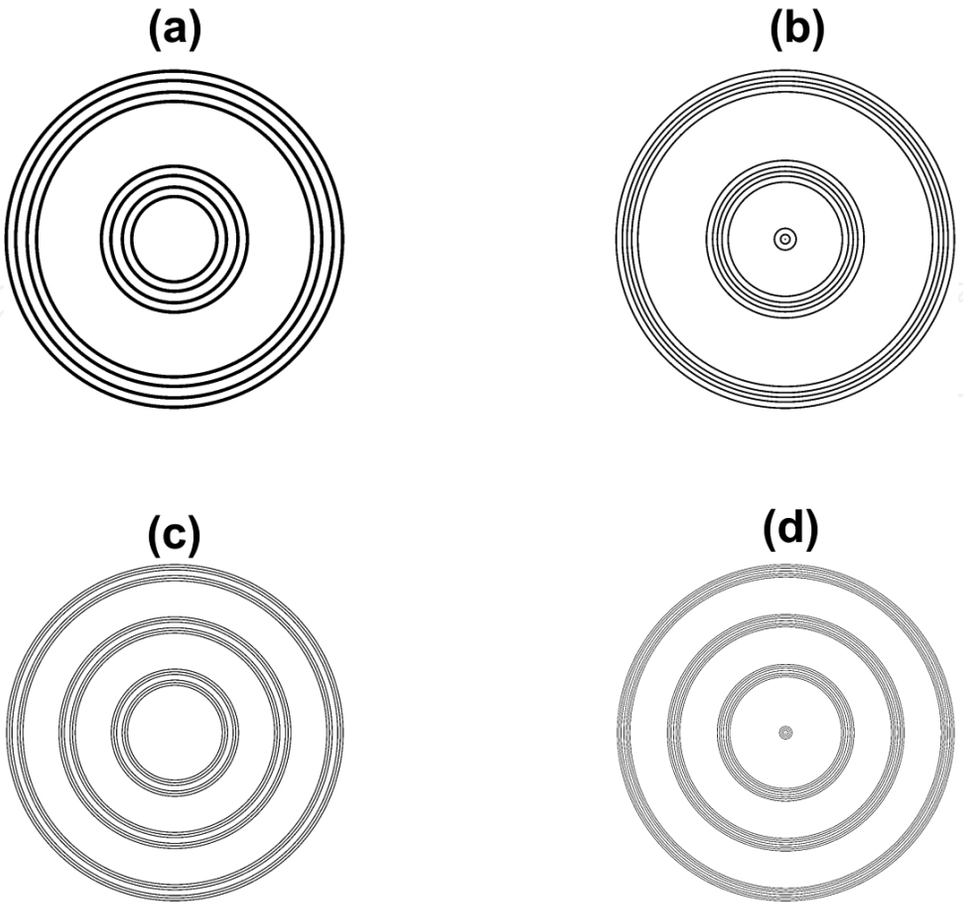


Figure 16. *XY*-plane view of the PCFL with f_{gc} = 0.4, D = 0.6, s = 2, and R = 12.5 cm and f = 100 kHz for (a) N = 4, (b) N = 5, (c) N = 6, and (d) N = 7.

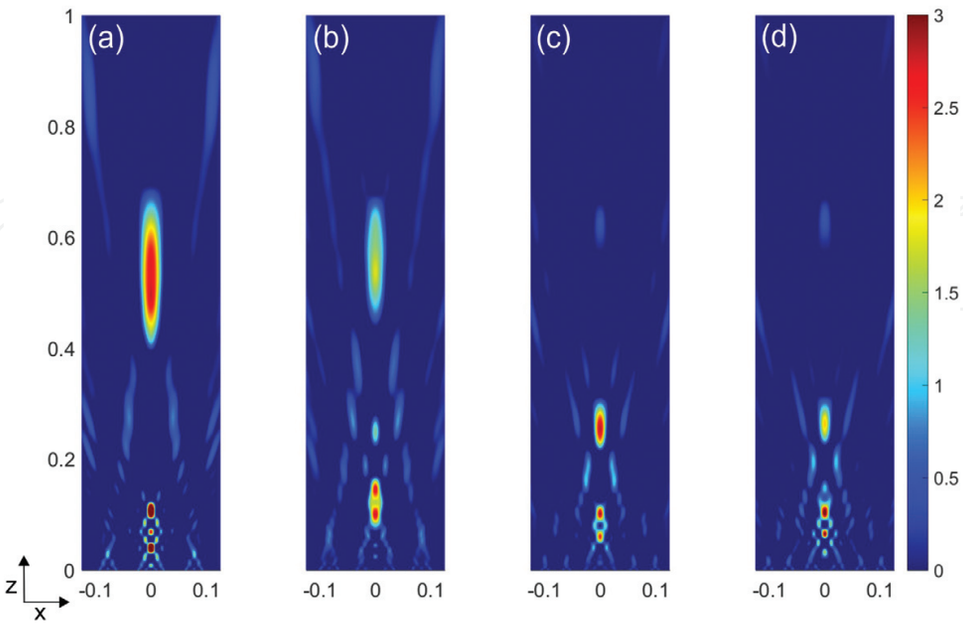


Figure 17. Two-dimensional spatial distribution of the acoustic gain (in dB) in the *XZ*-plane for the PCFL with f_{gc} = 0.4, D = 0.6, s = 2, and R = 12.5 cm parameters and working frequency of 100 kHz. The number of solid zones is: (a) N = 4, (b) N = 5, (c) N = 6, and (d) N = 7.

N	f_{gc}	r	$g_C/2R$	D
4	0.4	0.099	0.241	0.6
5	0.4	0.068	0.263	0.6
6	0.4	0.050	0.278	0.6
7	0.4	0.039	0.291	0.6

Table 1. Numerical results for variations of N.

4.5. Scalability of the lens

It this section the scalability of the lens is verified. This means that the same modulation of the acoustic beam is obtained, although at a different scale, when the size of the lens is reduced and the working frequency is increased in the same proportion. **Figure 18** shows the pressure in dBs along the Z-axis for four different lens sizes: (a) R = 12.5 cm, (b) R = 6.25 cm, (c) R = 3.125 cm, and (d) R = 1.5625 cm. The corresponding frequencies are: (a) 50, (b) 100, (c) 200, and (d) 400 kHz. As it can be observed from **Figure 18**, the pressure levels are equal for the different cases. The location of the focus area is scaled as expected. Notice that the horizontal axes in **Figure 14** show different scales. If the focus position is normalized with the size of the lens, the same results are obtained in all four cases.

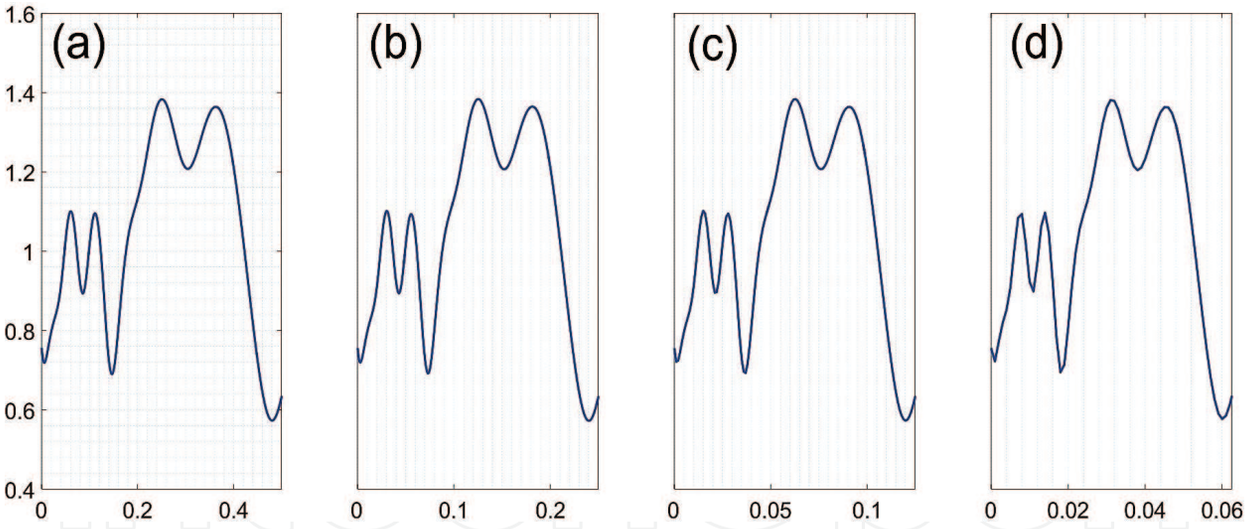


Figure 18. Spatial distribution of the acoustic pressure level (in dB) along the Z-axis or the PCFL with D = 0.6, N = 5, f_{gc} = 0.4, s = 2 for (a) R = 12.5 cm, (b) R = 6.25 cm, (c) R = 3.125 cm, and (d) R = 1.5625.

5. Conclusions

This work presents a comprehensive analysis of polyadic Cantor fractal lenses (PCFLs). It has been shown that the variation of the PCFL design parameters affect the modulation of the acoustic beam. Fractal dimension (D) affects the gain of the main focus of the pressure map. Varying the central gap fraction (f_{gc}) or the number of elements at stage s = 1 (N) results in a similar behavior, allowing to enhance the gain of further or closer foci, depending on the application requirements. Moreover, the numerical model shows that the PCFL is scalable.

Finally, once the PCFL is designed, a precise focus shifting along the *Z*-axis is achieved and controlled by slightly varying the working frequency. This gives the user a dynamic parameter to control the focus position without modifying the lens. This dynamic control is critical in certain medical applications where focusing of an ultrasonic beam allows tumors thermal ablation.

Acknowledgements

This work has been supported by Spanish MINECO (TEC2015-70939-R) and Generalitat Valenciana (AICO/2015/119).

Author details

Sergio Castiñeira-Ibañez[1], Daniel Tarrazó-Serrano[2], José Miguel Fuster[2], Pilar Candelas[2] and Constanza Rubio[2]*

*Address all correspondence to: crubiom@fis.upv.es

1 Electronic Engineering Department, University of Valencia, Burjassot, Valencia, Spain

2 Physical Technologies Center, Polytechnic University of Valencia, Valencia, Spain

References

[1] Mandelbrot BB. The Fractal Geometry of Nature. New York, USA: W.H. Freeman and Company; 1983. p. 468

[2] Takayasu H. Fractals in the Physical Sciences. Manchester, United Kingdom: Manchester University Press; 1990. p. 179

[3] Remón L, Calatayud A, Ferrando V, Giménez F, Furlan WD, Monsoriu JA. Fractal diffractive lenses. In: Shankar G. Pandalai, editors. Recent Research Developments in Optics. Vol. 8. Research Singpost; Kerala, India, 2013. pp. 31–71

[4] Petri A, Alippi A, Bettucci A, Cracium F, Farrelly F. Vibrational properties of a continuous self-similar structure. Physical Review B. 1994;49(21):15067–15075

[5] Sapoval B, Haeberlé O, Russ S. Acoustical properties of irregular and fractal cavities. Journal of the Acoustical Society of America. 1997;102(4):2014–2019. DOI: 10.1121/1.419653

[6] Lubniewski Z, Stepnowski A. Application of the fractal analysis in the sea bottom recognition. Archives of Acoustics. 1998; **23**(4):499–512

[7] Castiñeira-Ibáñez S, Romero-García V, Sánchez-Pérez JV, García-Raffi LM. Overlapping of acoustic bandgaps using fractal geometries. EPL. 2010;**92**:24007. DOI: 10.1209/0295-5075/92/24007

[8] Castiñeira-Ibáñez S, Rubio C, Romero-García V, Sánchez-Pérez JV, García-Raffi LM. Design, manufacture and characterization of an acoustic barrier made of multi-phenomena cylindrical scatterers arranged in a fractal-based geometry. Archives of Acoustics. 2012;**37**(4):455–462. DOI: 10.2478/v10168-012-0057-9

[9] Gomez-Lozano V, Uris A, Candelas P, Belmar F. Acoustic transmision through perforated plates with fractal subwavelength apertures. Solid State Communications. 2013;**165**:11–14. DOI: 10.1016/j.ssc.2013.04.012

[10] Saavedra G, Furlan WD, Monsoriu JA. Fractal zone plates. Optics Letters. 2003;**28**(12):971–973. DOI: 10.1364/OL.28.000971

[11] Monsoriu JA, Saavedra G, Furlan WD. Fractal zone plates with variable lacunarity. Optics Express. 2004;**12**(18):4227–4234. DOI: 10.1364/OPEX.12.004227

[12] Furlan WD, Saavedra G, Monsoriu JA. White-light imaging with fractal zone plates. Optics Letters. 2007;**32**(15):2109–2111. DOI: 10.1364/OL.32.002109

[13] Gimenez F, Monsoriu JA, Furlan WD, Pons A. Fractal photon sieve. Optics Express. 2006;**14**(25):11958–11963. DOI: 10.1364/OE.14.011958

[14] Monsoriu JA, Zapata-Rodriguez CJ, Furlan WD. Fractal axicons. Optics Communications. 2006;**263**(1):1–5. DOI: 10.1016/j.optcom.2006.01.020

[15] Jaggard AD, Jaggard DL. Scattering from fractal superlattices with variable lacunarity. Journal of the Optical Society of America A (Optics and Image Science). 1998;**15**(6):1626–1635. DOI: 10.1364/JOSAA.15.001626

[16] Aubert H, Jaggard DL. Wavelet analysis of transients in fractal superlattices. IEEE Transactions on Antennas and Propagation. 2002;**50**(3):338–345. DOI: 10.1109/8.999624

[17] Lehman M. Fractal diffraction grating built through rectangular domains. Optics Communications. 2001;**195**(1–4):11–26. DOI: 10.1016/S0030-4018(01)01285-8

[18] Mandelbrot BB. How long is the coast of Britain? Science. 1967;**156**:636–638

[19] Allain C, Cloitre M. Characterizing the lacunarity of random and deterministic fractal sets. Physical Review A. 1991;**44**:3552–3558. DOI: 10.1103/PhysRevA.44.3552

IntechOpen

IntechOpen